Volume 1 | Number 1 | Jan 2013 | Pages 1–100

Nanoscale

www.rsc.org/nanoscale

ROYAL SOCIETY OF CHEMISTRY

ROYAL SOCIETY OF CHEMISTRY

www.rsc.org/nanoscale

Journal Name

Nanoscale

ARTICLE TYPE

Structure and Catalytic Activities of Ferrous Center Confined on the Interface between Carbon Nanotube and Humic Acid

Bing Wang,[a] Xiaoyan Zhou,[a] Dongqi Wang,[a*] Jun-Jie Yin,[b] Hanqing Chen,[a] Xingfa Gao,[a] Jing Zhang,[c]
Kurash Ibrahim,[c] Zhifang Chai,[a,d] Weiyue Feng,[a*] and Yuliang Zhao[a,e]

Preparation of heterogeneous catalysts with active ferrous center is of great significance for industrial and environmental catalytic process. Nanostructured carbon materials (NCM), which possess free-flowing π electrons, can coordinate with transition metal, provide confinement environment for catalysis, and act as potential supports or ligand to construct analogous complex. However, designing such catalysts using NCM is still seldom studied to date. Herein, we synthesized a sandwich structured ternary complex *via* the coordination of Fe-loaded humic acid (HA) with C=C bond in aromatic ring of carbon nanotubes (CNTs), in which the O/N-Fe-C interface configuration provides confinement environment for ferrous site. The experimental and theoretical results revealed octahedrally/tetrahedrally coordinated geometry at Fe center and the strong hybridization between CNT C π^* and Fe 3d orbitals induces discretization of the atomic charges on aromatic ring of CNTs, which facilitates O_2 adsorption and electron transfer from carbon to O_2, thus enhances O_2 activation. The O_2 activation by the novel HA/Fe-CNT complex can be applied in the oxidative degradation of phenol red (PR) and bisphenol A (BPA) in aqueous media.

Introduction

Preparation of heterogeneous catalysts with ferrous active center is important for industrial and environmental catalysis because they can strongly absorb small gas molecules (such as O_2, NO, CO, CH_4, CO_2) and organic molecules, facilitate electron transfer and promote catalytic process.[1-4] These ferrous active sites are previously found in biological systems like heme Fe(II) enzyme (cytochromes P450) and non-heme Fe(II) enzymes (such as extradiol dioxygenases and Rieske dioxygenase), which can activate O_2 *via* an O_2 coordination to Fe(II) center, formation of O_2 adduct, and subsequent O-O bond cleavage.[5,6] In addition, the ferrous atom can keep those enzymes high reactivity and stability *via* confinement in nanosized space by various ensembles such as proteins (hemoglobin) and nanopore matrix (such as metal–organic frameworks).[7,8] Recent studies indicate that coordinately unsaturated ferrous can be confined at the interface between nanostructured transitional metal (TM: Fe, Co, Ni, etc.) oxide and precious metals (Pt/Au)[9] or on the surface of core-shell nanostructures (Cu@Pt),[10] which can help to activate O_2 and catalyze CO oxidation at low temperature. In those analogous ensembles, the geometric configuration and electronic structure contribute to the catalytic function of ferrous center. However, preparation of heterogeneous catalysts with active ferrous center is still a great challenge because of their complex and flexible structure.

The use of nanostructured carbon materials (NCMs) to stabilize the ferrous center is a currently unexplored yet highly promising. The NCMs, such as fullerene, carbon nanotubes (CNTs) and graphene, compose entirely of sp^2-hybridized carbon atoms and abundant free-flowing π electrons on surface, becoming potentially cheap, non-polluting and reusable heterogeneous catalysts in the development of modern sustainable green chemistry, and is expected to replace precious metal catalyst.[11,12] Additionally, NCMs, similar to carbene, π-alkene, and π-alkyne, may act as carbon π ligands to coordinate with transitional metals (TMs) in an η^1, η^2- or an η^6-mode, which may be used to design ferrous catalytic center *via* TM-C bond.[13-15] Furthermore, it has been reported that CNTs and fullerene, utilizing nanosized channels and cavities, provide intriguing confined environment for catalysts and reactants. Previous studies revealed that confinement inside CNTs facilitated the reduction of iron oxides[16-18] and iron nitride nanoparticles.[19] For instance, the reduced state of Fe_2O_3 and FeN nanoparticles (NPs) confined in CNTs have been identified as FeO, Fe, and Fe_xC_y phase for the Fe_2O_3 NPs;[18] and carbonitride (FeC_xN_{1-x} and $Fe_2C_xN_{1-x}$)[19] for the FeN ones under Fischer–Tropsch reaction conditions, which enhanced their catalytic activities.[20] Thus, the active ferrous site may be constrained on the surface of NCMs and possesses novel electronic properties and reactivities induced by their unique

Nanoscale Accepted Manuscript

coordination environment.

Herein, we utilize Fe-loaded humic acid (HA, $C_9H_9NO_6$) as ligands to interact with CNTs and synthesize a ternary sandwich-type HA/Fe-CNT complex, which can confine the active ferrous center at the interface between HA and CNTs. HA molecules possess rich oxygen/nitrogen-containing functional groups in the aromatic rings, thus can interact with CNTs *via* π-π stacking and provid coordination sites for iron cation as well. More importantly, HA is a naturally occurring organic substance, thus the complex HA/Fe-CNTs can be obtained on a large scale by facile, economical, and green strategies. The density functional theory (DFT) calculation shows that the ternary system (HA/Fe-CNT) possesses higher chemical stability than binary systems (CNT-Fe or HA-Fe). The synchrotron radiation X-ray absorption spectroscopy (XAS) studies reveal that the distorted octahedrally or tetrahedrally coordinated geometry contribute to the stabilization of ferrous site. The HA/Fe-CNT complex shows high catalytic activities for the activation of O_2 and H_2O_2, which can be applied in the oxidative degradation of phenol red (PR) and bisphenol A (BPA) in aqueous media.

Results and discussion

Synthesis of HA/Fe-CNT Sandwich-Type Complex

The preparation process of the HA/Fe-CNT is described in Scheme 1. To synthesize the HA/Fe-CNT, a well dispersed CNT-HA complex was prepared firstly to obtain high specific surface area for iron cation loading. Then ferric chloride solution was reacted with CNT-HA complex in water for 2 h at room temperature to form the ternary HA/Fe-CNT complex. In order to obtain efficient Fe loading into CNT-HA, the effects of the mass ratios of HA/CNT and the reaction pH conditions on CNT-HA formation were investigated. The synchrotron radiation based X-ray photoelectron spectroscopy (SR-XPS) analysis of C1s spectrum shows that the contents of C-OH, -C=O and -COOH in CNT-HA complex are related to HA/CNT mass ratio (Fig. S1, ESI). When the mass ratio of HA/CNT increased to 2:1, the contents of O-containing functional groups, including -OH, -C=O and -COOH, increased to 24.0%, 4.8% and 6.8%, respectively, which were beneficial for the Fe loading into CNT-HA *via* Fe-O coordination (Fig. S2, ESI). In addition, the contents of O-containing groups in CNT-HA complex ranged from 76.7% to 67.7% at pH 3.6-10.1, indicating that the CNT-HA had a potential to load Fe in a very wide pH range (Fig. S3, ESI).
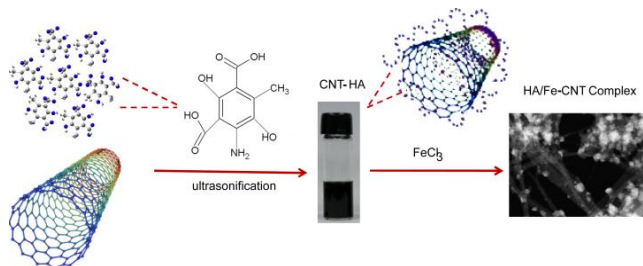
Scheme 1 Preparation process of HA/Fe-CNTs complex. HA/Fe-CNTs complex was prepared *via* the reaction of a well-dispersed CNT-HA suspension with ferric chloride solution at room temperature for 2 h and subsequent separation by centrifugation.

Physicochemical Characterization of HA/Fe-CNT Complex

We examined the morphology and structure of the obtained HA/Fe-CNT complex by high-resolution transmission microscopy (HRTEM) and scanning transmission electron microscope (STEM). The HRTEM image clearly presents the electron-dense precipitate on the CNT-HA surface (as arrow referred in Fig. 1a). The quantitative analysis by energy-dispersive X-ray spectroscopy (EDX) provided that the HA/Fe-CNT was composed of about 41.8 wt% of C, 6.5 wt% N, 8.2 wt% O, and 8.5 wt% Fe (Fig. 1b). Many strongly scattering iron cores, which were visible as dark or bright spots (corresponding to heavy elements), were observed in bright-field STEM (Fig. 1c) and the corresponding annular dark-field (ADF) images (Fig. 1d). These iron cores with a size of 5~10 nm were embedded in dense amorphous HA molecules and approached to the surface of CNTs, demonstrating that the sandwich-type HA/Fe-CNT complex was formed and iron cores was constrained at the interface between CNTs and HA. The iron cluster displays well-defined lattice fringes with a separation of 0.252 nm (Fig. 1e and 1f), which is close to the *d*-spacing of the lattice in Fe-O cluster compounds, such as (311) planes in cubic Fe_3O_4,[21] indicating the Fe-O bond character on the surfaces of CNTs.
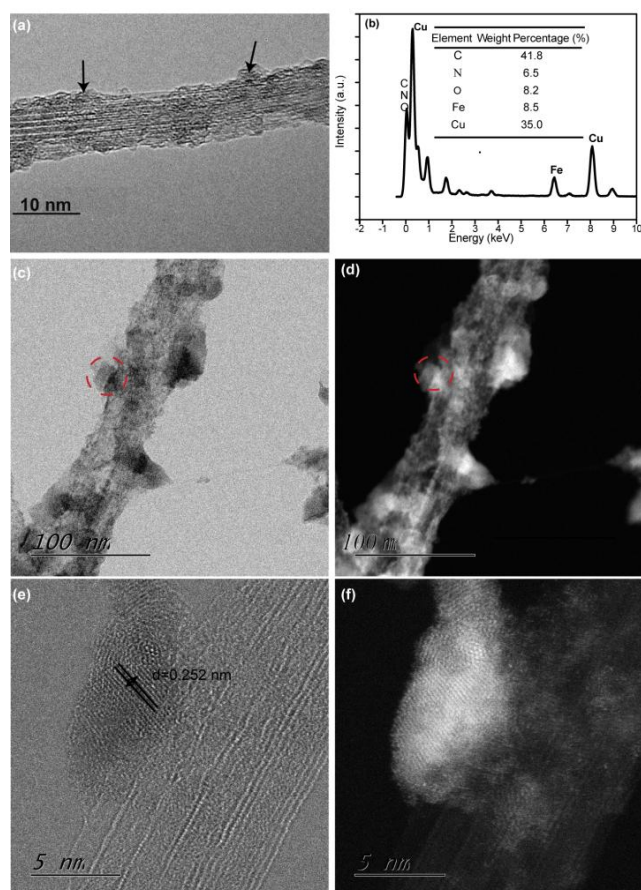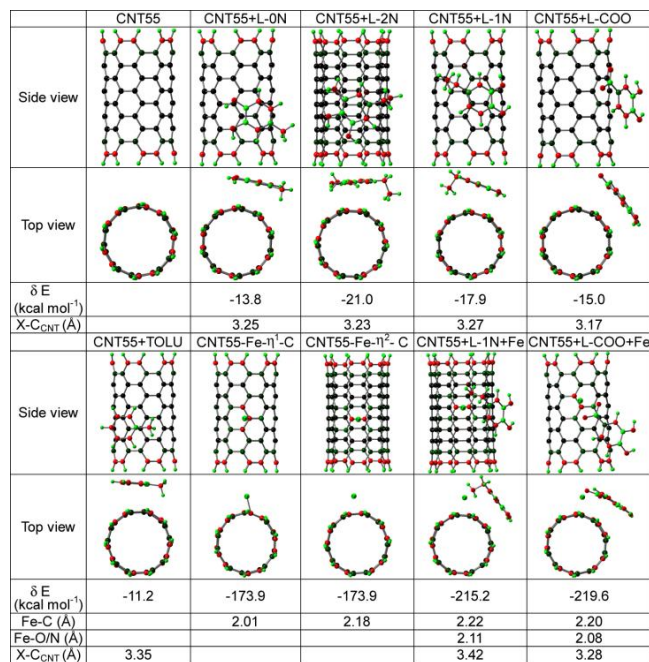
Fig. 1 Morphology and structure of HA/Fe-CNTs complex. HRTEM image (a) and EDX analysis (b) of HA/Fe-CNTs complex. Bright-field (c) and ADF STEM images (d) of HA/Fe-CNTs complex, (e and f) the lattices of iron cores marked by the red circle of (c) and (d).

Analysis of Structural Stability in HA/Fe-CNT Complex

The stability of the HA/Fe-CNT complex was assessed by DFT calculations with B97D method implemented in Gaussian 09.[22] (Fig. 2 & Fig. S4 in ESI). According to our calculations, in the binary system without Fe, the distances between the centroid of the phenyl ring of various ligands (L-1N, L-2N, L-COO) in HA and the closest C atom of CNT[5,5] are in the range of 3.17 – 3.35 Å, suggesting a π-π stacking interaction between them (Fig. 2). In binary system without HA, a naked Fe^{3+} cation may interact with the nanotube in an η^1- (residing on a C atom) or an η^2- (on a C-C bond) mode, rather than an η^6 one, with a Fe-C distance of 2.01 and 2.18 Å, respectively, of which the distance is shorter than the sum of their van der Waals radii.[14] In the ternary model system (Fig. 2), Fe^{3+} builds strong interaction with the functional groups of the organic ligand HA (2.11 Å for Fe-N in CNT55+L-1N+Fe and 2.08 Å for Fe-O in CNT55+L-COO+Fe). The coordination interaction between the electron-deficient Fe^{3+} and the electron-rich N or O atom may weaken the electron affinity of Fe^{3+}, leading to a decrease in the electrostatic interaction between Fe and CNT[5,5], as indicated by a longer distance between them. In addition, the interaction between Fe and CNT[5,5] and that between Fe and N/O of the ligand could modulate the orientation of the phenyl ring in HA, and the stable ternary model systems observed in our calculation are indeed originated from the composite effect of the inter-molecular interactions between the individual components.

The binding energies between the ligands and CNT[5,5] were calculated to be -11.2, -13.8, -17.9, -21.0, and -15.0 kcal/mol in CNT55+TOLU, CNT55+L-0N, CNT55+L-1N, CNT55+L-2N and CNT55+L-COO, respectively. For the ligands studied here, all contain polar groups except for toluene, and the smaller binding energy in CNT55+toluene indicates that the presence of polar groups may enhance the interaction between ligands and CNT[5,5], especially those with positively or negatively charged ones, e.g., $-NH_3^+$ and $-COO^-$. The binding energy of a naked Fe^{3+} cation to CNT[5,5] was calculated to be -173.9 kcal/mol. The presence of a charged ligand, L-COO here, brings further stabilization by 219.6-173.9-15.0=30.7 kcal/mol, suggesting the presence of HA may enhance the interaction between Fe^{3+} and a nanotube. The binding energy between HA-Fe and CNT were also calculated, which were -64.5 and -75.3 kcal/mol in COO-/Fe+CNT55 and N/Fe+CNT55, respectively. The high binding energy indicates that the formation of ternary HA/Fe-CNT complex is thermodynamically favourable, independent of the addition order.

	CNT55	CNT55+L-0N	CNT55+L-2N	CNT55+L-1N	CNT55+L-COO
Side view					
Top view					
δ E (kcal mol^{-1})		-13.8	-21.0	-17.9	-15.0
X-C$_{CNT}$ (Å)		3.25	3.23	3.27	3.17
	CNT55+TOLU	CNT55-Fe-η^1-C	CNT55-Fe-η^2- C	CNT55+L-1N+Fe	CNT55+L-COO+Fe
Side view					
Top view					
δ E (kcal mol^{-1})	-11.2	-173.9	-173.9	-215.2	-219.6
Fe-C (Å)		2.01	2.18	2.22	2.20
Fe-O/N (Å)				2.11	2.08
X-C$_{CNT}$ (Å)	3.35			3.42	3.28

X: the centroid of the phenyl ring of the ligand.

Fig. 2 Theoretical calculation of CNT, HA, and Fe interactions in HA/Fe-CNTs complex. Top and side views of intermolecular interactions in the binary system (CNT-HA and CNT-Fe) and ternary system (CNT-HA-Fe). The binding energies and the distance between the ligand of humic acid and the closest C atom of CNT were indicated.

Activation of O_2 and H_2O_2 by HA/Fe-CNT Complex

In order to identify the ability of the novel HA/Fe-CNT complex to serve as a catalyst for the activation of O_2 and H_2O_2 in aqueous media, an electron paramagnetic resonance (EPR) in conjunction with spin trapping techniques was performed, using the 1-hydroxy-3-carboxy-pyrrolidine (CPH) and 5,5-dimethyl-1-pyrroline N-oxide (DMPO) as superoxide anion radical ($O_2^{\cdot-}$) and hydroxyl radical ($^\cdot$OH) spin probes, respectively. No obvious EPR signals were observed in CNT-HA and CNT-Fe substances. When iron-loaded HA (HA-Fe) and HA/Fe-CNT were added, the $O_2^{\cdot-}$ and $^\cdot$OH signal intensity increased significantly. It has been reported that HA-Fe may reduce O_2 to $O_2^{\cdot-}$ and H_2O_2 to $^\cdot$OH via Fenton or Haber-Weiss reactions.[23-25] Herein, though the amount of HA-Fe (1.6 mg) was four times that of HA/Fe-CNT (0.4 mg) to be used, the production of $O_2^{\cdot-}$ and $^\cdot$OH by HA/Fe-CNT complex was about 2.5- and 1.7-fold increase, demonstrating the enhanced one-electron reduction of O_2 and H_2O_2 into $O_2^{\cdot-}$ and $^\cdot$OH by HA/Fe-CNT, respectively (Fig. 3).[23] The catalytic activities of the complex for H_2O_2 activation are equivalent to that of the heterogeneous Fenton catalysts, such as Fe_2O_3, Fe_2O_3, and Fe_3O_4 NPs, which are the most powerful catalysts for H_2O_2 activation that have ever been reported.[26,27]
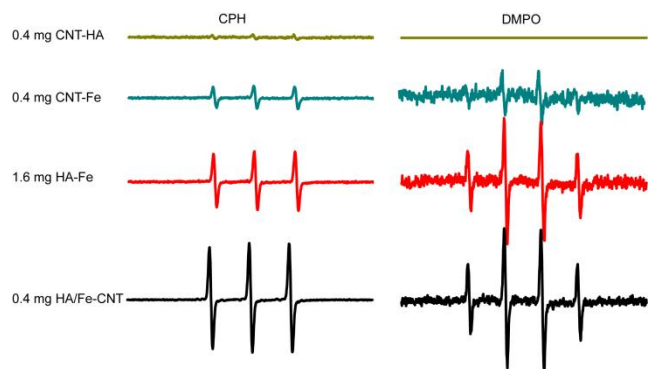
Fig. 3 Enhanced activation of O₂ (a) and H₂O₂ (b) by HA/Fe-CNTs complex. Generation of O₂·⁻ and ·OH in binary (CNT-HA, CNT-Fe, and HA-Fe) and ternary (HA/Fe-CNT) aqueous systems was measured using CPH and DMPO as their spin probes, respectively. All EPR spectra were measured at 20 mW microwave power, 100 G scan range and 1 G field modulation. All of the chemical agents used in EPR experiments were purchased from Sigma-Aldrich, USA.

Mechanism of O₂ Activation by HA/Fe-CNT Complex

The adsorption of O₂ molecule to catalysts has been speculated to be a rate-determined step in O₂ activation.[28,29] Many studies indicated that the ferrous center in non-heme Fe(II) [*e.g.*, NHFe(II)) enzymes, heme-containing proteins, and metal-organic complexes, could act as O₂ adsorption sites, in which cosubstrates or organic ligands allow Fe(II) coordination unsaturation and leaving an open coordination site for O₂ binding.[30] In the study, the formation of ferrous center in HA/Fe-CNT complex was demonstrated by SR-XPS and XAS techniques. The SR-XPS analysis shows the presence of Fe 2p peaks (Fig. 4a,b), which are deconvoluted into Fe(II) 2p$_{3/2}$ (710.8 eV), Fe(II) 2p$_{1/2}$ (723.8 eV), Fe(III) 2p$_{3/2}$ (712.2 eV) and Fe(III) 2p$_{1/2}$ (725.0/726.5 eV), indicating the co-existence of Fe(II) and Fe(III) states in HA/Fe-CNT complex.[31] The quantitative analysis of XPS suggests that about 44.9% of Fe exist as Fe(II) species in HA/Fe-CNT complex (Table S1). The X-ray absorption near-edge structure spectra (XANES) of Fe K-edge indicates that the pre-edge 1s → 3d peak of HA/Fe-CNT possesses a similar centroid position and shape to that of the Fe(II)-containing species (*e.g.*, FeN, FeO and Fe₃C in Fig. 4c and 4d line a), which have a wide pre-edge peak at 7111.8 ~ 7112.4 eV and shift left 1.4 ~ 2.0 eV relevant to the Fe(III) species (*e.g.*, FeCl₃ and Fe₂O₃ in Fig. 4d, line b). The extended X-ray absorption fine structure (EXAFS) oscillations of Fe K-edge revealed a prominent peak located at R = 1.6 Å, corresponding to the first shell of Fe-C/O/N coordination (Fig. 4e). The C K-edge XANES spectrum shows a pronounced broadening and a low-energy shoulder (284.5 eV) of C=C 1s → π* (Fig. 4f, line a), suggesting a strong hybridization between CNT C π* and Fe 3d orbitals. The best-fit to the first shell of HA/Fe-CNT yields a Fe-O bond distance of 1.93 Å and Fe-C of 2.09 Å; and the coordination numbers are 3.88 for Fe-O (from two H₂O molecule and one carboxylate group) and 2.02 for Fe-C, which are consistent with the six-coordinated Fe model with four Fe-O and two Fe-C coordination (Fig. 5a and 5b). While, the best-fit also proposes a tetrahedrally coordinated Fe complex with one Fe–N bond (2.01 Å), one Fe-C (2.24 Å), and two water molecules (Fig. 5a and 5b). The shorter Fe-O/N/C distance obtained by EXAFS than that from the DFT calculation might be related with the distortion of the octahedral or tetrahedral geometry induced by

steric effects among the aromatic ligand of bulk CNT and N/O ligands of HA.[32] It has been known that Fe(II) active site has a higher affinity to O₂ than to H₂O molecule, thus the position of two very weakly bonded H₂O molecule may become the site of O₂ binding as well as the dissociation of intermediate, resulting in the O₂ activation.[33,34] However, the detailed structure change of HA/Fe-CNT complex during O₂ activation is still unclear and needs to be further explored.
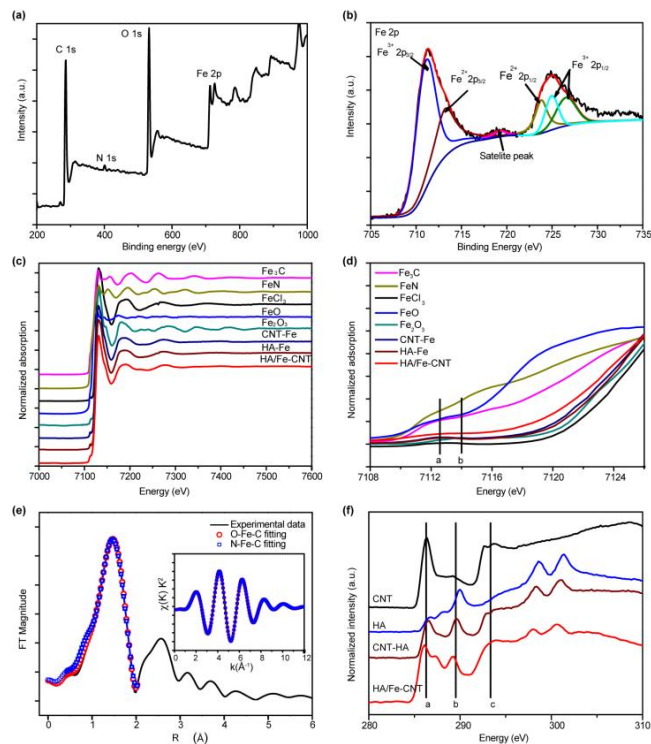

Fig. 4 Electronic structure of Fe and C in ternary HA/Fe-CNTs complex and corresponding binary (CNT-Fe, HA-Fe or CNT-HA) or unary system. The XPS survey spectrum (a) and Fe 2p XPS (b) in HA/Fe-CNT complex; (c and d) Fe K-edge XAS spectra and pre-edge region of the chemical standards (Fe₃C, FeN, FeCl₃, FeO and Fe₂O₃), binary (CNT-Fe and HA-Fe) and ternary system (HA/Fe-CNT); Fourier transform of the k²χ(K) EXAFS spectra of HA/Fe-CNT complex (e) and C K-edge XANES spectra in CNT, HA, CNT-HA, and HA/Fe-CNT complex (f).

The effective electron transfer from carbon π electron to adsorbed O₂ is another key factor for O₂ activation. The strong donor effects from ligands at ferrous center (such as NHFe(II) enzymes) are also beneficial for electron transfer from the ligand to iron cation.[6] According to the C K-edge XANES spectra, a strong hybridization between CNT C π* and Fe 3d orbitals occurs, which is beneficial for charge redistribution between them.[35] The DFT calculation further indicates that the O/N-Fe-C configuration induces a discretization of the aromatic ring charges on CNTs and presents dipoles in such conjunctions (Fig. 5c and Fig. 6). The carbon atoms involved in Fe-C π bonding possess a partial negative charge due to its polarization by the Fe³⁺ cation; in the meantime, the adjacent C atoms possess substantially high density positive charge (Fig. 5c and Fig.6). The O/N-Fe-C geometric configuration and the large extent of charge delocalization in CNT55+L-COO+Fe and CNT55+L-N+Fe (Fig. 5c) can facilitate the electron transfer from CNT to Fe ion and

subsequently transfer to the adsorbed O_2, thus contributing to O_2 activation (Fig. 5c).[36-38]

(a)

First-shell EXAFS fitting results for Fe in HA/Fe-CNT complex

	Shell	N per Fe atom	R (Å)	σ^2(Å^2)	R (%)
O -Fe -C	Fe -O	3.88 ± 0.18	2.01	0.011	0.1
	Fe -C	2.02 ± 0.14	2.29	0.001	
N -Fe -C	Fe -N	0.95 ± 0.28	2.01	0.011	0.2
	Fe -C	0.93 ± 0.30	2.24	0.013	

N: coordination number; R: bond length; σ^2: Debye Waller factors; R: parameter for quality of fit
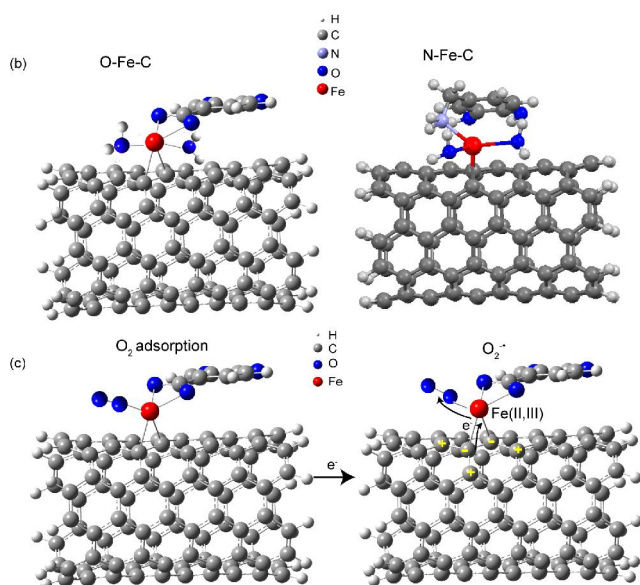
Fig. 5 Structure parameters of HA/Fe-CNTs catalyst and mechanism of O₂ activation. (a) The structural parameters and (b) geometry of HA/Fe-CNTs catalyst; (c) mechanism of O₂ activation by HA/Fe-CNTs.
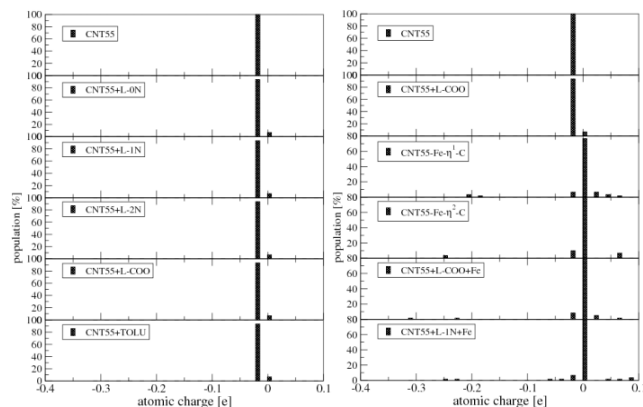
Fig. 6 Population of atomic charges of the inner region of the carbon nanotube. The fluctuation of atomic charges of a carbon nanotube upon the binding of ligand and/or Fe^{3+} cation.

Oxidative Degradation of Phenol Red and Bisphenol A

Aqueous heterogeneous activation of O_2 and H_2O_2 can be applied in a wide range of fields, such as oxidative degradation of organic pollutants in wastewater. We investigated the oxidative

degradation of phenol red (PR) and bisphenol A (BPA) in aqueous media by the novel HA/Fe-CNT catalyst. The results showed that the PR was oxidized to benzoquinone-like substance at pH 4.1 ~ 10.1 by HA/Fe-CNT catalysis, while no oxidized PR products was observed in the presence of only CNTs, or CNT-HA, CNT-Fe, and HA-Fe (Fig. S5a,b, ESI). The decrease of PR in CNT+PR and CNT-HA+PR solutions was due to the adsorption by CNT and CNT-HA. In the CNT-Fe system, in consistent with the theoretical calculation, the low stability of CNT-Fe make them inefficient catalysis for PR oxidation. Similarly, HA/Fe-CNT showed catalytic activity for oxidative degradation of BPA into open ring or hydroxylated complex, which were identified by liquid chromatography-mass spectrometry (LC-MS, Fig. S5c and 5d, ESI). The catalytic degradation reaction of BPA follows the first order kinetics with a rate constant of 0.47 min^{-1} (Fig. S5e, ESI), which was about 10- to 100-fold faster than those by the most effective methods, such as heterogeneous Fenton-based reactions (using H_2O_2 as oxidant) or iron nanoparticle-based catalytic reactions.[39,40] After 3-times running-cycles, the recovery of HA/Fe-CNT can still reach about 70% (Fig. S6, ESI), showing the high efficient and reusable capability of the catalyst.

Experimental section

Materials

Highly purified (> 95%) carbon nanotubes were supplied from Chengdu Organic Chemicals Co. Ltd., Chinese Academy of Sciences. These nanotubes were synthesized using a chemical vapor deposition (CVD) method with mean diameter of 2 nm. HA (purity > 99.0%) and $FeCl_3 \cdot 6H_2O$ (AR, > 99.0%) were purchased from Alfa Aesar and Beijing Chemical Reagents Company, respectively. Phenol red (AR, > 99.0%) and Bisphenol A （> 99.0%) were purchased from Alfa Aesar and TCI Development Co. Ltd (Shanghai, China), respectively.

Synthesis of HA/Fe-CNT Complex

A dissolved stock solution (1000 mg/L) of HA was prepared in ultrapure Milli-Q water *via* magnetic stirring for 10 h and gradual dilution to the tested concentrations. The CNT-HA complex was prepared *via* dispersing CNTs in HA solution by sonication for 2 h at 15-17 °C in ice bathing, and then centrifugation to remove free HA molecules. Finally, 4 µL ferric chloride solution (2×10^5 mg/L) was added to the CNT-HA solution and the reaction was carried out for 2 h at room temperature to form the ternary HA/Fe-CNT complex following centrifugation to remove free iron ion.

Characterization of HA/Fe-CNT Complex

The HRTEM images of HA-Fe-CNT were collected with a JEOL JSM-2100 electron microscope operating at 120 kV. The surface functional groups of the tested complex were characterized by SR-XPS. The XPS measurements were performed at 4B9B beamline in Beijing Synchrotron Radiation Facility (BSRF, Beijing, China) equipped with a Si(111) double crystal monochromator. The core level spectra, including C 1s, O 1s, and N 1s were recorded at the incident photon energy of 500 eV with a step size of 0.16 eV, using a hemispherical electron energy

analyzer (HA150, VSW) with energy resolution better than 300 meV. The XPS spectra of Fe 2p were recorded at the incident photon energy of 950 eV with a step size of 0.32 eV.

ADF and bright-field STEM images were performed at an aberration-corrected STEM (JEM-ARM 200F) equipped with a cold field-emission electron source and double C_S correctors for the condenser lens and objective lens. The STEM images were collected at an operating voltage of 200 kV.

The Fe K-edge XAS spectra were recorded from 50 eV below to 700 eV above the Fe K-edge threshold energy (7112 eV) using a Lytle detector in fluorescence mode at 1W1B beamline in BSRF. The Fe XAS spectra of Fe-containing chemical standards, including $FeCl_3$, Fe_3C, FeN, FeO, and Fe_2O_3 powders, were measured in a transmission mode (using a N_2/Ar gas-filled ionization chamber). The C K-edge XANES spectra of the tested samples were acquired at the BSRF 4B7B beamline and the data were recorded with the total electron yield (TEY) method. The XAS data analysis of Fe and C is described in the ESI.

Theoretical Calculation

In order to understand the intermolecular interactions in the ternary system containing carbon nanotube (CNT), humic acid (HA) and iron (Fe) cations in water solvent, simplified models have been prepared and fully optimized using DFT with dispersion interaction taken into account empirically (B97D).[41] The solvent effect was taken into account using a continuum SMD model,[42] and the binding distance and binding energy in binary systems (CNT-HA and CNT-Fe) and ternary system (HA-Fe-CNT) were compared. All structures reported here have been fully optimized at the level of B97D/6-31G(d),[41,43-46] and the nature of the each geometry was confirmed to be a minimum by vibrational analysis. The calculation details based on DFT are described in the ESI.

EPR Measurement

All EPR measurements were carried out using a Bruker EMX EPR Spectrometer (BrukerBiospin, Billerica, MA). The production of $O_2^{\cdot-}$ and $^{\cdot}OH$ was measured using the CPH and DMPO as their respective spin probes. The EPR experiments are described in detail in the ESI.

Oxidative Degradation of PR and BPA

The HA/Fe-CNT catalysts were added in PR or BPA solution (pH 7.0) and the reaction was carried out at 25 °C for 2, 4, 8, 12, 24, 48 h, then samples were centrifuged at 10,000 rpm for 30 min. The supernatants of PR and BPA were detected by UV-Visible spectra (Spectra Max M2). The degraded products of BPA were analyzed by the ultra-performance liquid chromatography system (UPLC, Waters, USA) connected to electrospray ionization-tandem mass spectrometry (Micro TOF-QII, Bruker Daltonics). The operating conditions of UPLC-ESI-MS are described in the ESI. The recovery and recycling capability of HA/Fe-CNT were recorded after 3-times recycling catalysis of PR and the PR oxidative products were analyzed.

Conclusions

In summary, we describe a strategy to confine ferrous active site on the interface between CNTs and HA using HA loaded Fe to coordinate with aromatic rings of CNTs. The higher binding energy in HA/Fe-CNT system and shorter Fe-C, and Fe-N/O bond distance in HA/Fe-CNT complex than binary system (CNT-HA and CNT-Fe) revealed the stability of HA/Fe-CNT complex. This synthesized sandwich-type nanostructured CNT-based catalysts possess high catalytic activities for the activation of O_2 and H_2O_2. The distorted octahedral or tetrahedral geometry play important roles in the stabilization of Fe(II) center and O_2 adsorption. The strong hybridization between CNT C π^* and Fe 3d orbitals induces the discretization of the atomic charges of aromatic ring of CNTs, which facilitates the electron transfer from carbon to O_2 *via* metal ion, thus favors O_2 activation. The O_2 activation by the novel HA/Fe-CNT complex can be applied in the oxidative degradation of organic pollutants (*e.g.*, phenol red and bisphenol A) in aqueous media.

Notes and references

[a] CAS Key Laboratory for Biomedical Effects of Nanomaterials and Nanosafety, CAS Key Laboratory of Nuclear Radiation and Nuclear Energy Technology, Institute of High Energy Physics, Chinese Academy of Sciences, Beijing 100049, China
[b] Division of Analytical Chemistry, Office of Regulatory Science, Center for Food Safety and Applied Nutrition, US Food and Drug Administration, College Park, MD, USA
[c] Beijing Synchrotron Radiation Facility, Institute of High Energy Physics, Chinese Academy of Sciences, Beijing 100049, China
[d] School of Radiation Medicine and Protection, Soochow University, Suzhou, 215123, China
[e] CAS Key Laboratory for Biomedical Effects of Nanomaterials and Nanosafety, National Center for Nanoscience and Technology of China, Beijing 100190, China

† Electronic Supplementary Information (ESI) available: [Optimization of the mass ratios of HA to CNTs and the reaction pH conditions for Fe loading; scanning electron microscope (SEM), UV-Vis-near-infrared, Raman spectroscopy, Fourier transform infrared spectroscopy (FTIR) for CNT-HA; EPR experiment and UPLC-ESI-MS analysis; and DFT calculation].

1. H. Chen, K. B. Cho, W. Lai, W. Nam, and S. Shaik, *J. Chem. Theory Comput.*, 2012, **8**, 915-926.
2. Q. Fu, F. Yang, and X. H. Bao, *Acc. Chem. Res.*, 2013, **46**, 2725-2739
3. D. B. Garagorri, I. Lagoja, L. F. Veiros, and K. A. Kirchner, *Dalton Trans.*, 2011, **40**, 4778-4792.
4. D. J. Xiao, E. D. Bloch, J. A. Mason, W. L. Queen, M. R. Hudson, N. Planas, J. Borycz, A. L. Dzubak, P. Verma, K. Lee, F. Bonino, V. Crocella`, J. Yano, S. Bordiga, D. G. Truhlar, L. Gagliardi, C. M. Brown, and J. R. Long, *Nat. Chem.*, 2014, **6**, 590-595.
5. L. Jr. Que and W. B. Tolman, *Nature*, 2008, **455**, 333-340.
6. K. M. Light, J. A. Hangasky, M. J. Knapp, and E. I. Solomon, *Dalton Trans.*, 2014, **43**, 1505-1508.
7. Y. K. Hwang, D. Y. Hong, J. S. Chang, S. H. Jhung, Y. K. Seo, J. Kim, A. Vimont, M. Daturi, C. Serre, and G. Férey, *Angew. Chem. Int. Ed.*, 2008, **47**, 4144-4148.
8. J. Liu, L. Chen, H. Cui, J. Zhang, L. Zhang, and C.Y. Su, *Chem. Soc. Rev.*, 2014, **43**, 6011-6061.

9. Q. Fu, W. X. Li, Y. Yao, H. Liu, H. Y. Su, D. Ma, X. K. Gu, L. Chen, Z. Wang, H. Zhang, B. Wang, and X. H. Bao, *Science*, 2010, **328**, 1141-1144 .

10. X. Guo, Q. Fu, Y. Ning, M. Wei, M. Li, S. Zhang, Z. Jiang, and X. H. Bao, *J. Am. Chem. Soc.*, 2012, **134**, 12350-12353.

11. Y. Zhao, L.Yang, S. Chen, X. Wang, Y. Ma, Q. Wu, Y. Jiang, W. Qian, and Z. Hu, *J. Am. Chem. Soc.*, 2013, **135**, 1201-1204.

12. J. P. Paraknowitsch and A. Thomas, *Energy Environ. Sci.*, 2013, **6**, 2839-2855.

13. H. J. Himmel, *Nat. Chem.*, 2013, **5**, 88-89.

14. F. Nunzi, F. Mercuri, A. Sgamellotti, and N. Re, *J. Phys. Chem. B.*, 2002, **106**, 10622-10633.

15. D. Devarajan, T. B. Gunnoe, and D. H. Ess, *Inorg. Chem.*, 2012, **51**, 6710-6718.

16. W. Chen, X. Pan, M. G. Willinger, D. S. Su, and X. Bao, *J. Am. Chem. Soc.*, 2006, **128**, 3136-3137.

17. W. Chen, X. Pan, and X. Bao, *J. Am. Chem. Soc.*, 2007, **129**, 7421-7426.

18. W. Chen, Z. Fan, X. Pan, and X. Bao, *J. Am. Chem. Soc.*, 2008, **130**, 9414-9419.

19. S. Guo, Z. Yang, X. Pan, J. Wang, and X. Bao, *Energy Environ. Sci.*, 2011, **4**, 4500-4503.

20. X. Pan and X. Bao, *Chem. Commun.*, 2008, 6271-6281.

21. Z. Liu, B. Lv, D. Wu, Y. Sun, and Y. Xu, *Particuology*, 2013, **11**, 327-333.

22. Gaussian 09, Revision D.01, M. J. Frisch, G. W. Trucks, H. B. Schlegel, G. E. Scuseria, M. A. Robb, J. R. Cheeseman, G. Scalmani, V. Barone, B. Mennucci, G. A. Petersson, H. Nakatsuji, M. Caricato, X. Li, H. P. Hratchian, A. F. Izmaylov, J. Bloino, G. Zheng, J. L. Sonnenberg, M. Hada, M. Ehara, K.Toyota, R. Fukuda, J. Hasegawa, M. Ishida, T. Nakajima, Y. Honda, O. Kitao, H. Nakai, T. Vreven, J. A. Jr. Montgomery, J. E. Peralta, F. Ogliaro, M. Bearpark, J. J. Heyd, E. Brothers, K. N. Kudin, V. N. Staroverov, R. Kobayashi, J. Normand, K. Raghavachari, A. Rendell, J. C. Burant, S. S. Iyengar, J. Tomasi, M. Cossi, N. Rega, J. M. Millam, M. Klene, J. E. Knox, J. B. Cross, V. Bakken, C. Adamo, J. Jaramillo, R. Gomperts, R. E. Stratmann, O. Yazyev, A. J. Austin, R. Cammi, C. Pomelli, J. W. Ochterski, R. L. Martin, K. Morokuma, V. G. Zakrzewski, G. A. Voth, P. Salvador, J. J. Dannenberg, S. Dapprich, A. D. Daniels, O. Farkas, J. B. Foresman, J. V. Ortiz, J. Cioslowski, and D. J. Fox, Gaussian, Inc., Wallingford CT, **2009**.

23. M. D. Paciolla, E. A. Ghabbour, G. Davies, and S. A. Jansen, *Environ. Sci. Technol.*, 1999, **33**, 1814-1818.

24. V. Prabhakaran, C. G. Arges, and V. Ramani, *Proc. Natl. Acad. Sci. U. S. A.*, 2012, **109**, 1029-1034.

25. J. M. Noel, A. Latus, C. Lagrost, E. Volanschi, and P. Hapiot, *J. Am. Chem. Soc.*, 2012, **134**, 2835-2841.

26. B. Wang, J. J. Yin, X. Y. Zhou, K. Ibrahim, Z. F. Chai, Y. L. Zhao, and W. Y. Feng, *J. Phys. Chem. C.*, 2013, **117**, 383-392.

27. M. A. Voinov, J. O. S. Pagan, E. Morrison, T. I. Smirnova, and A. I. Smirnov, *J. Am. Chem. Soc.*, 2011, **133**, 35-41.

28. J. Cho, S. Jeon, S. A. Wilson, L. V. Liu, E. A. Kang, J. J. Braymer, M. H. Lim, B. Hedman, K. O. Hodgson, J. S. Valentine, E. I. Solomon, and W. Nam, *Nature*, 2011, **478**, 502-505.

29. A. P. Woodham, G. Meijer, and A. Fielicke, *J. Am. Chem. Soc.*, 2013, **135**, 1727-1730.

30. M. Y. M. Pau, J. D. Lipscomb, and E. I. Solomon, *Proc. Natl. Acad. Sci. USA*, 2007, **104**, 18355-18362.

31. A. P. Grosvenor, B. A. Kobe, M. C. Biesinger, and N. S. McIntyre, *Surf. Interface Anal.*, 2004, **36**, 1564-1574.

32. S. J. George, B. M. Barney, D. Mitra, R. Y. Igarashi, Y. Guo, D. R. Dean, S. P. Cramer, and L. C. Seefeldt, *J. Inorg. Biochem.*, 2012, **112**, 85-92.

33. S. Ye, X. Wu, L. Wei, D. Tang, P. Sun, M. Bartlam, and Z. Rao, *J. Biol. Chem.*, 2007, **282**, 3391-3402.

34. T. E. Westre, P. Kennepohl, J. G. DeWitt, B. Hedman, K. O. Hodgson, and E. I. Solomon, *J. Am. Chem. Soc.*, 1997, **119**, 6297-6314.

35. B. J. Schultz, C. Jaye, P. S. Lysaght, D. A. Fischer, D. Prendergast, and S. Banerjee, *Chem. Sci.*, 2013, **4**, 494-502.

36. Z. Wang, B. Yang, Y. Wang, Y. Zhao, X. M. Cao, and P. Hu, *Phys. Chem. Chem. Phys.*, 2013, **15**, 9498-9502.

37. P. Zhang, B. B. Xiao, X. L. Hou, Y. F. Zhu, and Q. Jiang, *Sci. Rep.*, 2014, **4**, 3821.

38. X. B. Hu, Y. T. Wu, H. R. Li, and Z. B. Zhang, *J. Phys. Chem. C.*, 2010, **114**, 9603-9607.

39. W. Wang, Y. Liu, T. L. Li, and M. H. Zhou, *Chem. Eng. J.*, 2014, **242**, 1-9.

40. Y. H. Huang, C. C. Su, Y. P. Yang, and M. C. Lu, *Environ. Prog. Sustainable Energy*, 2013, **32**, 187-192.

41. S. Grimme, *J. Comp. Chem.*, 2006, **27**, 1787-1799.

42. A. V. Marenich, C. J. Cramer, and D. G. Truhlar, *J. Phys. Chem. B.*, 2009, **113**, 6378-6396.

43. R. Ditchfield, W. J. Hehre, and J. A. Pople, *J. Chem. Phys.*, 1971, **54**, 724-728.

44. W. J. Hehre, R. Ditchfield, and J. A. Pople, *J. Chem. Phys.*, 1972, **56**, 2257-2261.

45. M. M. Francl, W. J. Pietro, W. J. Hehre, J. S. Binkley, D. J. DeFrees, J. A. Pople, and M. S. Gordon, *J. Chem. Phys.*, 1982, **77**, 3654-3665.

46. V. A. Rassolov, J. A. Pople, M. A. Ratner, and T. L. *J. Chem. Phys.*, 1998, **109**, 1223-1229.

Nanoscale Accepted Manuscript

Entry for the Table of Contents
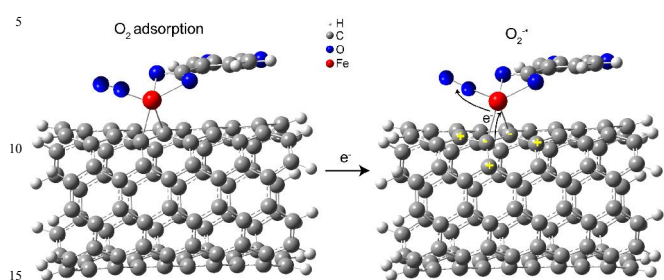
A sandwich-type CNT-based catalyst was synthesized, in which the discretization of the atomic charges on aromatic ring of CNTs induced by octahedral or tetrahedral geometry at ferrous center and strong hybridization between CNT C π^* and Fe 3d orbitals enhanced O_2 activation.